



## Original Paper

## Measurement of pore diffusion factor of porous solid materials

Jin-Tao Guo <sup>a, b, 1</sup>, Ya-Qian Wei <sup>a, 1</sup>, Sheng-Li Chen <sup>a, \*</sup>, Wei Sun <sup>a</sup>, Ting-Ting Fan <sup>a</sup>,  
Ming-Ri Xu <sup>a</sup>, Chang-Cheng Zhang <sup>a</sup>

<sup>a</sup> State Key Laboratory of Heavy Oil Processing, and Department of Chemical Engineering, China University of Petroleum-Beijing, Beijing, 102249, China

<sup>b</sup> Petrochemical Research Institute of PetroChina Company Limited, Daqing, 163000, Heilongjiang, China



## ARTICLE INFO

## Article history:

Available online 14 April 2022

Edited by Xiu-Qiu Peng

## Keywords:

Porous materials  
Well-defined and uniform pore structure materials  
Internal diffusion  
Diffusion factor  
Tortuosity

## ABSTRACT

Internal diffusion of molecules in porous materials plays an important role in many chemical processes. However, the pore diffusion capacity of porous materials cannot be measured by conventional catalyst characterization methods. In the present paper, a pore diffusion factor, the ratio of the diffusion-constriction factor to the pore tortuosity of the porous materials, was proposed to measure the diffusion ability of pores inside solid materials, and a method was proposed for measuring the diffusion factor using a well-defined and uniform pore size material as a reference. The diffusion factor was calculated based on the effective diffusion coefficients and the diffusion-constriction factor and pore tortuosity of the reference porous materials. The pore diffusion factor measurement can be performed at room temperature and atmospheric pressure. The pore diffusion factor of conventional porous materials was found to be much smaller than 1, indicating that there is a lot of room for improving the diffusion ability of the conventional catalysts and adsorbents, and could be significantly increased through adding small number of fibers into the conventional porous materials as template.

© 2022 The Authors. Publishing services by Elsevier B.V. on behalf of KeAi Communications Co. Ltd. This is an open access article under the CC BY-NC-ND license (<http://creativecommons.org/licenses/by-nc-nd/4.0/>).

## 1. Introduction

Internal diffusion of molecules in porous materials plays an important role in many chemical processes, such as adsorption processes (Neves et al., 2021; Rao et al., 2021), solid catalytic reaction processes (Peng et al., 2020; Chen et al., 2007). In the case of adsorption processes, the adsorption rate is usually controlled by the internal diffusion rate of molecules in porous materials. For solid catalytic reaction process, when the diffusion rate of reaction molecules in catalyst pores is smaller than the reaction rate, the overall reaction rate is controlled by internal diffusion and can be improved by increasing the diffusion rate of reaction molecules. Actually, many catalytic processes are controlled by catalyst internal diffusion. For example, the hydrogenation of heavy oil is a typical reaction process controlled by diffusion within the catalyst (Absi-Halabi et al., 1995; Li et al., 1995). As a consequence, it is of wide and great significance to study the pore diffusion factor of porous materials.

Effective diffusion coefficient ( $D_e$ ) is usually used to measure the diffusion ability of molecules inside porous materials. The  $D_e$  of a molecule in porous materials can be expressed as (Fogler, 2006) Eq. (1)

$$D_e = \frac{D_B \cdot \epsilon \cdot f}{\tau} \quad (1)$$

Where,  $D_B$  is the bulk diffusion coefficient of molecules, and it depends on chemical process system and operation conditions, is independent of the porous materials and has a fixed value for a specific system.  $\epsilon$ ,  $f$  and  $\tau$  are the porosity, the diffusion-constriction factor and the tortuosity of the porous materials, respectively. The  $\epsilon$  is easy to be accurately measured by, for example, the low temperature  $N_2$  adsorption, mercury porosimetry and water wetting methods (ISO/TC 24/SC 4, ISO 15901-2:2006; ISO/TC 24/SC 4, ISO 15901-3:2007; Liu, 1990).

It seems that  $D_e$  can be easily calculated using Eq. (1). Actually, it's not the case, because both  $f$  and  $\tau$  are very difficult to be accurately measured. It is generally accepted that  $f$  is related to the ratio of diffusion molecule's size to the diameter of pores (Renkin, 1954; Wang et al., 2014; Beck and Schults, 1970). Because the conventional catalyst is not uniform in pores, containing a variety of

\* Corresponding author.

E-mail addresses: [sichen@cup.edu.cn](mailto:sichen@cup.edu.cn), [shenglichen62@163.com](mailto:shenglichen62@163.com) (S.-L. Chen).

<sup>1</sup> These authors contributed equally to this research work.

different sizes and shapes of pores, and what is more, the pore size has significant effect on the effective diffusion coefficient (Chen et al., 1994; Chang et al., 1998; Kobayashi et al., 1987), hence the  $f$  of conventional catalysts is actually almost immeasurable and unknowable. So is the tortuosity  $\tau$ .

There are mainly three methods for measuring the tortuosity  $\tau$ , namely the steady state method (Gao et al., 1997a), the dynamic diffusion method, also known as SPSRM chromatography (Gao et al., 1997b), and the pressure gradient method (Wyllie and Gregory, 1955). However, one cannot obtain the accurate value of  $\tau$  by these methods.

In the steady-state method, the diffusion in porous materials is carried out in a diffusion pool (Gao et al., 1997a). The diffusion pool is divided into an upper (or left) diffusion chamber and a lower (or right) diffusion chamber, separated by the porous materials to be tested. The upper diffusion chamber and the lower diffusion chamber are purged with two different gases in a certain flow rate, and the gas components are diffused through the catalyst pellet from one diffusion chamber to another. The  $D_e$  and  $\tau$  of the catalyst can be obtained by analyzing the composition of the gas flowing out of the two chambers. In this method it is assumed that the porous materials have a uniform pore size, and that the all pores are cylindrical and connected to the surface of the porous materials. In fact, the pore size of the porous materials is not uniform (there are large pores and small pores), and the pores of the porous materials have random shape, not cylindrical, and some of the catalyst pores are not connected to the surface of the catalyst. Therefore, the tortuosity  $\tau$  cannot be accurately measured by the steady-state method.

For the dynamic diffusion method (Gao et al., 1997b), in order to measure the pore tortuosity, the porous materials are loaded into a column in a string, and tracers are injected into the column at different carrier gas flows. Adsorption and desorption occur when the tracer flows through the column with carrier gas. The effective diffusion coefficient is calculated according to the broadening of the tracer chromatographic peak, and then the pore tortuosity is calculated. This method also assumes that the pore size of the porous materials is uniform, and that the pore of the catalyst is cylindrical. However, the pore size of the actual catalyst is neither uniform nor cylindrical, so the measured pore tortuosity is also unreliable.

In the pressure gradient method (Wyllie and Gregory, 1955; Comiti and Renaud, 1989), the pressure drop generated by the liquid flowing through the porous materials to be tested is measured to determine the pore tortuosity. The larger the pore tortuosity, the greater the pressure gradient. This method is only valid for measuring the pore tortuosity of through-pores and large-pore materials; hence it cannot be used for measuring the pore tortuosity of conventional porous materials, which has a variety of different sizes and shapes of pores.

As a conclusion, because the pores of conventional porous materials are not fully connected, nor uniform in diameter, and the pore structure is different from one site to the other in the porous materials, both the constriction factor and the tortuosity of porous materials are immeasurable.

Here in this paper, the constriction factor and the tortuosity are lumped into one factor, called the pore diffusion factor ( $\beta$ ), and it is set to equal to  $f/\tau$ . We measured the  $\beta$  of several conventional porous  $\gamma$ -Al<sub>2</sub>O<sub>3</sub> by determining the effective diffusion coefficient of porous  $\gamma$ -Al<sub>2</sub>O<sub>3</sub> and comparing it with that of a reference porous material which has well-defined and uniform pore size. The pore diffusion factor of conventional porous  $\gamma$ -Al<sub>2</sub>O<sub>3</sub> was found to be much smaller than 1, indicating that there is a lot of room for improving the diffusion ability of the conventional porous

materials, and could be significantly increased through adding small number of fibers into the conventional porous materials as template.

## 2. The theory of measurement of the pore diffusion factor

For the reference porous material, Eq. (1) becomes,

$$D_{e0} = \frac{D_B \cdot \varepsilon_0 \cdot f_0}{\tau_0} \quad (2)$$

Where,  $D_{e0}$ ,  $\varepsilon_0$ ,  $f_0$  and  $\tau_0$  are the effective diffusion coefficient, the porosity, the diffusion-constriction factor and the tortuosity of the reference porous material, respectively.

The reference porous material was fabricated through ordered packing of monodisperse silica spheres (Face-centric cubic (FCC) structure). Because the monodisperse silica spheres is uniform, the pore structure of the reference porous material is uniform and well defined. By using large silica spheres, we can increase the pore size of the reference porous material. When the pores are large enough, the diffusion of molecules in pores reaches free diffusion or bulk diffusion, so that the diffusion-constriction factor  $f_0$  would be equal to 1. Because the pore's structure of the model catalyst is well defined, the pore tortuosity can be calculated geometrically, and it was found to be  $\pi/2$  for the opal materials (Sun et al., 2019). The pore's tortuosity of porous materials formed through packing of spherical particle was also obtained by pressure drop measurements (Comiti and Renaud, 1989), and it was found as follows,

$$\tau = 1 + 0.41 \ln(1/\varepsilon) \quad (3)$$

Considering the  $\varepsilon$  of perfect FCC material is 0.26, the  $\tau$  value of FCC material calculated by Eq. (3) is very similar to its geometrical value of  $\pi/2$ .

From Eq. (1) and Eq. (2), setting  $f_0 = 1$ , we can get

$$\beta = \frac{f}{\tau} = \frac{D_e}{D_{e0}} \frac{\varepsilon_0}{\varepsilon} \frac{1}{\tau_0} \quad (4)$$

As long as a well-defined and uniform pore size material is used as a reference material, we can obtain the pore diffusion factor of a porous materials by measuring their effective diffusion coefficients. It's important to point out that the calculation of  $\beta$  is independent of  $D_B$ . The  $D_e$  and  $D_{e0}$  may vary with temperature, while their ratio ( $D_e/D_{e0}$ ) is independent of temperature. That is, the effective diffusion coefficient measurement does not need to be carried out under the actual operation (reaction or adsorption) conditions, but can be carried out at room temperature, making the  $\beta$  measurement much more convenient.

Dynamic adsorption-diffusion method was used to determine the effective diffusion coefficient of molecules in porous materials. Fig. 1 is a schematic diagram of solute A diffusion in a spherical porous pellet.

Assuming the adsorption between A molecules in pore fluid and the molecules adsorbed on the pore surface of catalyst reaches its adsorption equilibrium, and the adsorption amount is proportional to concentration  $C_A$  in pore fluid, we have

$$q_A = kC_A \quad (5)$$

Where  $q_A$  is the amount of A adsorbed on the surface of pores, mol/cm<sup>2</sup>;  $k$  is the coefficient of isotherm Eq. (5).

A diffusion model of molecule A in the spherical porous pellet is established based on the material balance (Sun et al., 2019).

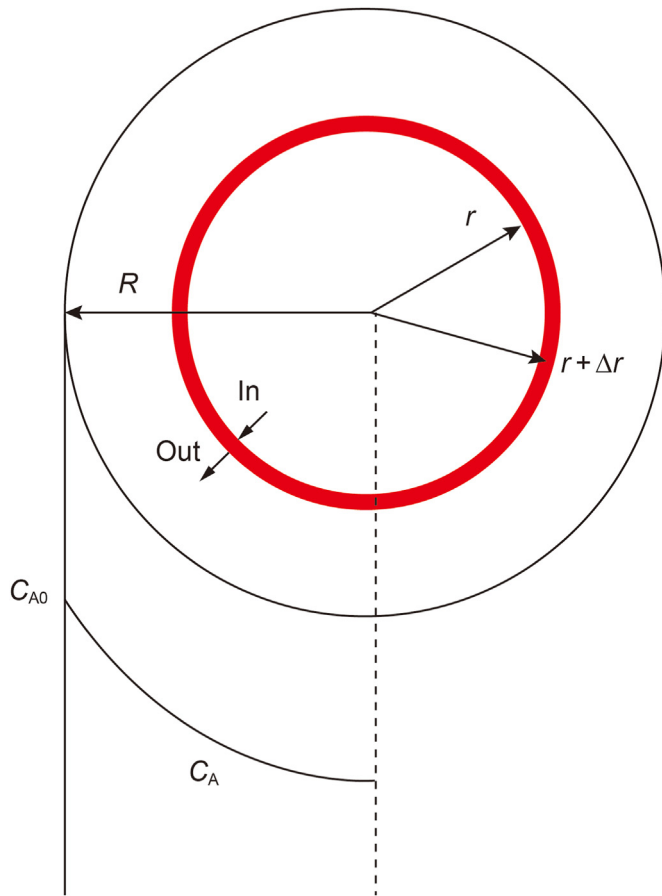


Fig. 1. Schematic diagram of solute A diffusion in a spherical porous pellet.

$$D_e \frac{1}{r^2} \frac{\partial}{\partial r} \left( r^2 \frac{\partial C_A}{\partial r} \right) = [\varepsilon + (1 - \varepsilon)S \cdot \rho_s \cdot k] \frac{\partial C_A}{\partial t} \quad (6)$$

Where  $C_A(r, t)$  is the concentration of solute A in pores at the radius  $r$  of the sphere pellet at time  $t$ ,  $\text{mg}/\text{cm}^3$ ,  $S$  is the specific surface area,  $\rho_s$  is the solid skeleton density of the spherical porous pellet,  $\text{g}/\text{cm}^3$ .

When the amount of solute A adsorbed in the porous material is negligible in compared with the total amount of solute A in the solution, the concentration of solute A in the solution does change during the adsorption. If external diffusion resistance outside the particle is much smaller than internal diffusion resistance inside the particle, the concentration of solute A on the outside surface of the porous pellet is constant and equals to that in the bulk solution,  $C_{A0}$ . In this case, the initial and boundary conditions for Eq. (6) are

$$\begin{cases} t = 0, & 0 \leq r < R, & C_A = 0 \\ \{ t \geq 0, & r = 0, & \frac{dC_A}{dr} = 0 \\ t \geq 0, & r = R, & C_A = C_{A0} \end{cases} \quad (7)$$

Letting  $u_1 = C_A/C_{A0}$  and  $x = r/R$ , equation (6) can be rewritten as follows,

$$[\varepsilon + (1 - \varepsilon) \cdot S \cdot \rho_s \cdot k] \frac{\partial u_1}{\partial t} = \frac{D_e}{R^2} \frac{1}{x^2} \frac{\partial}{\partial x} \left( x^2 \frac{\partial u_1}{\partial x} \right) \quad (8)$$

The initial and boundary conditions for Eq. (8) are rewritten as Eq. (9):

$$\begin{cases} t = 0, & 0 \leq x < 1, & u_1 = 0 \\ \{ t \geq 0, & x = 0, & \frac{du_1}{dx} = 0 \\ t \geq 0, & x = 1, & u_1 = 1 \end{cases} \quad (9)$$

The uptake  $M_t$  of A in the spherical catalyst pellet at time  $t$  can be calculated with Eq. (10).

$$\begin{aligned} M_t &= \int_0^R C_A 4\pi r^2 \varepsilon dr + \int_0^R q_A 4\pi r^2 (1 - \varepsilon) \cdot \rho_s \cdot S dr \\ &= 4\pi \varepsilon R^3 C_{A0} \int_0^1 u_1 x^2 dx + 4\pi (1 - \varepsilon) R^3 \cdot \rho_s \cdot S \cdot k \cdot C_{A0} \int_0^1 u_1 x^2 dx \end{aligned} \quad (10)$$

The equilibrium uptake  $M_\infty$  is calculated with Eq. (11).

$$\begin{aligned} M_\infty &= \int_0^R C_{A0} 4\pi r^2 \varepsilon dr + \int_0^R q_{A0} 4\pi r^2 (1 - \varepsilon) \rho_s S dr \\ &= \frac{1}{3} 4\pi \varepsilon R^3 C_{A0} + \frac{1}{3} 4\pi (1 - \varepsilon) R^3 \rho_s S k C_{A0} \end{aligned} \quad (11)$$

The adsorption uptake rate is defined as the ratio of the uptake  $M_t$  at time  $t$  to the equilibrium uptake  $M_\infty$ :

$$\frac{M_t}{M_\infty} = 3 \int_0^1 u_1 x^2 dx \quad (12)$$

The partial differential Eq. (8) with boundary conditions of Eq. (9) can be solved by numerical method. The effective diffusion coefficient  $D_e$  can be obtained through optimizing the parameter  $D_e$  in Eq. (8) by using MATLAB software.

### 3. Experimental

#### 3.1. Materials

Dibenzothiophene (DBT), n-octane, 1,3,5-tritoluene, ethyl-orthosilicate (TEOS), aqueous ammonia and methanol used in this work were all pure reagents. Soft wood fibers, the average diameter and length of which were  $\sim 24 \mu\text{m}$  and  $\sim 1.8 \text{mm}$  respectively, were obtained from a paper factory.

#### 3.2. Conventional porous solid materials

Alumina ( $\gamma\text{-Al}_2\text{O}_3$ ) is one of the most widely used catalyst supports and adsorbents, therefore it was used as the conventional porous solid materials here in this paper. Four kinds of  $\gamma\text{-Al}_2\text{O}_3$  pellets were used as porous materials, which were prepared by adding the soft wood fibers into a same  $\gamma\text{-Al}_2\text{O}_3$  powder during catalyst forming. The fibers were removed from the  $\gamma\text{-Al}_2\text{O}_3$  pellets through calcination of the samples at  $550^\circ\text{C}$  for 3 hrs. The  $\gamma\text{-Al}_2\text{O}_3$  pellets prepared using 1.0 wt%, 2.0 wt%, and 3.0 wt% fiber as template were designated as  $\text{Al}_2\text{O}_3\text{-1}\%$ ,  $\text{Al}_2\text{O}_3\text{-2}\%$  and  $\text{Al}_2\text{O}_3\text{-3}\%$  respectively. The controller sample without any fiber template was designated as  $\text{Al}_2\text{O}_3\text{-0}\%$ .

#### 3.3. Preparation of the reference porous material

Firstly, the 300 nm monodisperse silica spheres were synthesized through hydrolysis and condensation of TEOS using the silica



sol (Ludox, AS-40) as seeds via seeded growth method (Chen et al., 1996; Chen, 1998). Then silica opal materials were fabricated through ordered packing of the monodisperse silica spheres in a beaker under the gravity force. After that, the silica opal materials were calcined at 700 °C for 2 h to solidify the silica opal materials. Finally, solidified silica opal materials were hydrothermally treated at 180 °C for 5 h to hydroxylate the silica surface. In order to convert the SiO<sub>2</sub> surface into Al<sub>2</sub>O<sub>3</sub> surface, the silica opal materials were put into 25% Al(NO<sub>3</sub>)<sub>3</sub> aqueous solution at 80 °C for 12 h, rinsed with DI H<sub>2</sub>O, and calcined 500 °C for 5 h. The Al<sub>2</sub>O<sub>3</sub> modification process was performed twice to completely convert the silica surface of silica opal materials into Al<sub>2</sub>O<sub>3</sub> surface. Because only 1–2 atomic layers of Al<sub>2</sub>O<sub>3</sub> were lain on the surface of the silica opal materials, the Al<sub>2</sub>O<sub>3</sub>-modified silica opal, i.e. the reference porous material, kept the silica opal's defined and uniform pore structure of its mother silica opal materials (Zhou et al., 2013). The reference porous material as prepared was designated as Al<sub>2</sub>O<sub>3</sub>/SiO<sub>2</sub> Opal.

### 3.4. Characterization of the porous materials

The BET specific surface area and pore size distribution of the porous materials were determined by low temperature N<sub>2</sub> adsorption-desorption method using ASAP-2420 physical adsorption apparatus at the temperature of 77 K. The pore volume of porous material was measured by water absorption method. The morphology of the catalyst was observed by using scanning electron microscope (SEM) of FEI Quanta200 F, with the operation acceleration voltage being 20 kV.

### 3.5. Measurement of effective diffusion coefficient

The adsorption solution, containing octane (50 wt%), 1,3,5-trimethylbenzene (50 wt%) and 2,6-dimethyl pyridine (1000 ppm) as the solvent, and DBT as the solute, was used for the diffusion experiments. The diffusion experiments were carried out at room temperature (25 °C).

Above of all, the adsorption equilibrium equation (Eq. (5)) was obtained. A fixed amount of porous pellets was put into a beaker which containing enough adsorption solution so that the concentration kept unchanged after the adsorption, and then the beaker was vibrated on a shaker at 120 rpm. After the adsorption reached its equilibrium, the porous pellets were taken out of the beaker, washed with the solvent (50 wt% 1,3,5-trimethylbenzene, 50 wt% octane, 1000 ppm 2,6-dimethyl pyridine) for several times, until all the DBT adsorbed was washed out of the catalyst pellets. The washing solvent was collected and the DBT concentration of it was determined by the UV-Vis spectrophotometry method using UV-1800s UV-vis spectrophotometer at wavelength 327 nm. The total amount of DBT washed out of the catalyst pellets minus the amount of DBT in the solution in the catalyst pores is the amount of DBT adsorbed on the surface of the catalyst pores. Five solutions with the DBT concentration being 1000 ppm, 3000 ppm, 5000 ppm, 7000 ppm and 9000 ppm were used to obtain the adsorption equilibrium equation.

The diffusion solution containing 5000 ppm DBT was used for the measurement of effective diffusion coefficient. The procedures for determination of DBT adsorption take-up are similar to that of

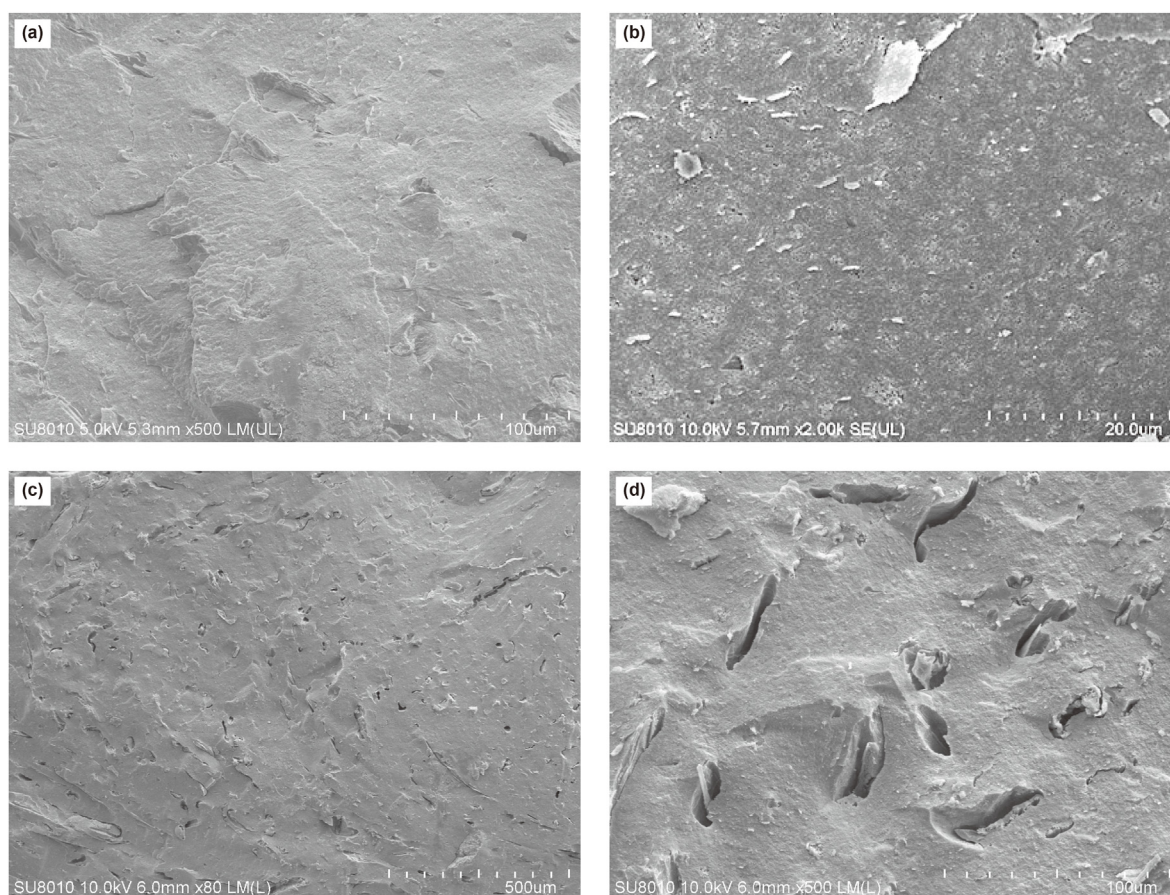


**Fig. 2.** The SEM image of the prepared porous  $\gamma$ -Al<sub>2</sub>O<sub>3</sub> ((a) and (b) : porous  $\gamma$ -Al<sub>2</sub>O<sub>3</sub> prepared without template; (c) and (d) : porous  $\gamma$ -Al<sub>2</sub>O<sub>3</sub> prepared with 3 wt% fiber as template).

experiment described above for the determination of the adsorption equilibrium equation. A fixed amount of porous pellets was first saturated with the solvent, and then added into a beaker containing the diffusion solution. The beaker was vibrated on the shaker at 120 rpm, which is fast enough to eliminate catalyst pellet external diffusion resistance. A part of the porous pellets was taken out of the beaker at a desired time and washed with the solvent. The amount of DBT in the washing solvent was also measured by UV-Vis spectrophotometry method with the UV-1800s UV-vis spectrophotometer.

#### 4. Results and discussions

Fig. 2 is the SEM image of the outside surface of the prepared porous  $\gamma$ - $\text{Al}_2\text{O}_3$  pellets. It is clear that in comparison with the  $\gamma$ -

**Table 1**  
The pore structure characteristics of the prepared the porous  $\gamma$ - $\text{Al}_2\text{O}_3$ .

$\gamma$ - $\text{Al}_2\text{O}_3$ samples	Porosity	Pore volume, mL/g	Specific surface area, $\text{m}^2/\text{g}$
$\text{Al}_2\text{O}_3$ -0%F	0.660	0.566	326.1
$\text{Al}_2\text{O}_3$ -1%F	0.653	0.551	319.5
$\text{Al}_2\text{O}_3$ -2%F	0.654	0.554	324.6
$\text{Al}_2\text{O}_3$ -3%F	0.655	0.554	318.4
$\text{Al}_2\text{O}_3/\text{SiO}_2$ Opal	0.29	0.22	13.47

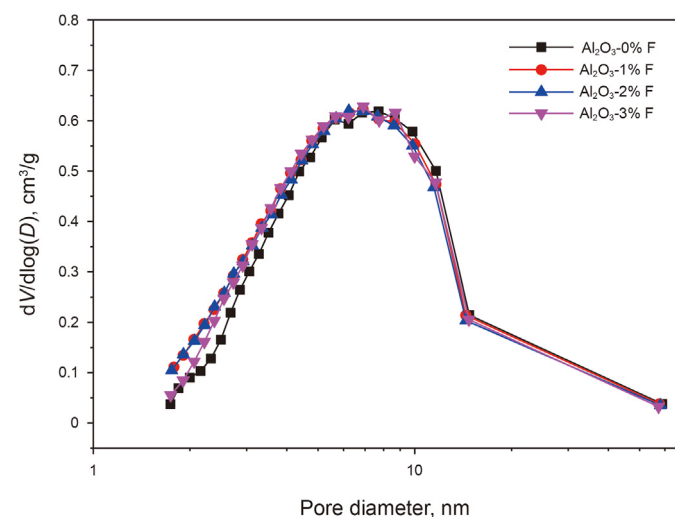


Fig. 3. Pore size distribution of the prepared porous  $\gamma$ - $\text{Al}_2\text{O}_3$  pellets.

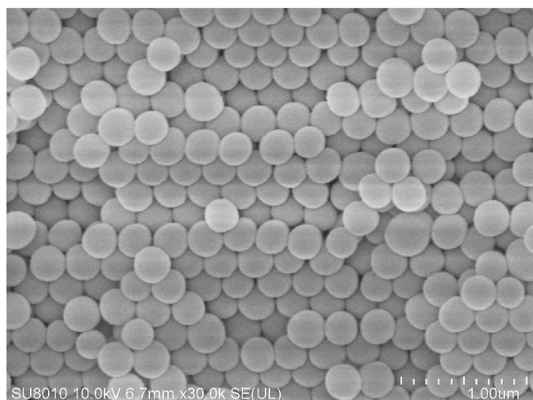


Fig. 4. SEM image of the reference solid porous materials ( $\text{Al}_2\text{O}_3/\text{SiO}_2$  Opal).

$\text{Al}_2\text{O}_3$  pellets formed without any template, the  $\gamma$ - $\text{Al}_2\text{O}_3$  pellets prepared with 3.0 wt% fibers have large pores created by burning the fibers in the  $\gamma$ - $\text{Al}_2\text{O}_3$  pellets. The pore structure characteristics, measured by the classic low temperature  $\text{N}_2$  adsorption-desorption method at the temperature of 77 K, of all the prepared porous  $\gamma$ - $\text{Al}_2\text{O}_3$  pellets are shown in Table 1, and the pore size distribution are shown in Fig. 3. It can be seen that although different amounts of fibers are used as template during the porous  $\gamma$ - $\text{Al}_2\text{O}_3$  pellets forming, the characteristics of the obtained  $\gamma$ - $\text{Al}_2\text{O}_3$ , including the pore porosity, pore volume, specific surface area and the pore size distribution, are almost identical to each other. Although the fibers used as template was less than 3.0 wt%, because the fibers having the length of about 1.6 mm can connect  $\text{Al}_2\text{O}_3$  pellets pores, the  $\text{Al}_2\text{O}_3$  pellets pores should be more communicated than that of the controller sample. Table 1 and Fig. 3 show that the classic low temperature  $\text{N}_2$  adsorption-desorption method, almost the only method for people to characterize solid materials pore structure reported in literature, is not able to tell the difference in pore structure for the internal diffusion.

Fig. 4 is the SEM of the surface morphology of the  $\text{Al}_2\text{O}_3/\text{SiO}_2$  Opal used as the reference solid porous materials. As shown in Fig. 4, the  $\text{Al}_2\text{O}_3/\text{SiO}_2$  Opal pellets were composed of very uniform microspheres, and the pore structure of which should be well-

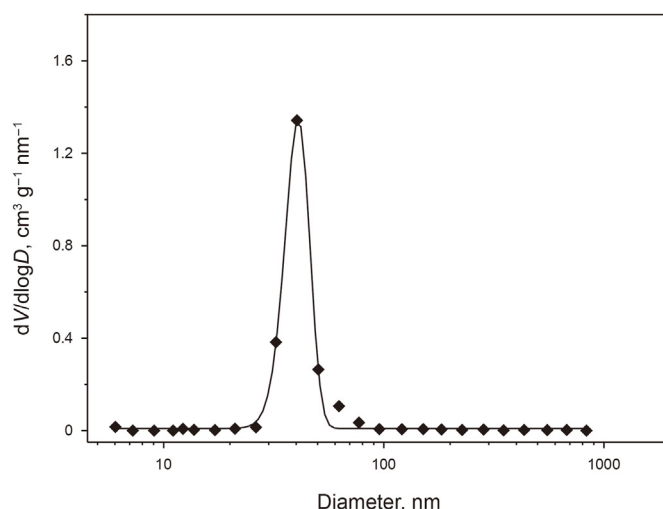


Fig. 5. Pore size distribution of the reference solid porous materials ( $\text{Al}_2\text{O}_3/\text{SiO}_2$  Opal).

**Table 2**  
The surface adsorption equilibrium constant ( $k$ ) of  $\text{Al}_2\text{O}_3$  pellets and the reference porous solid.

Catalysts	$k$ , $10^{-7}$ cm
$\text{Al}_2\text{O}_3$ -0%F	3.212
$\text{Al}_2\text{O}_3$ -1%F	3.626
$\text{Al}_2\text{O}_3$ -2%F	3.895
$\text{Al}_2\text{O}_3$ -3%F	3.534
$\text{Al}_2\text{O}_3/\text{SiO}_2$ Opal.	1.939

**Table 3**  
The effective diffusion coefficient of porous solid pellets.

porous solid	$D_e$ , $10^{-6}$ $\text{cm}^2/\text{s}$
$\text{Al}_2\text{O}_3$ -0%F	1.27
$\text{Al}_2\text{O}_3$ -1%F	1.38
$\text{Al}_2\text{O}_3$ -2%F	1.57
$\text{Al}_2\text{O}_3$ -3%F	1.76
$\text{Al}_2\text{O}_3/\text{SiO}_2$ Opal.	3.02



defined and uniform. The pore size distribution obtained by low temperature N<sub>2</sub> adsorption-desorption, as shown in Fig. 5, shows that the Al<sub>2</sub>O<sub>3</sub>/SiO<sub>2</sub> Opal pellets was uniform in pore size. Because the pores inside the Al<sub>2</sub>O<sub>3</sub>/SiO<sub>2</sub> Opal pellets are the caves between the monodisperse microspheres ordered packed, these pores are fully communicated with each other and to the outside surface. In the contrary, many pores inside the conventional  $\gamma$ -Al<sub>2</sub>O<sub>3</sub> pellets cannot communicate to the outside surface, as was mentioned in the introduction.

Five solutions, with the DBT concentrations of 1000 ppm, 3000 ppm, 5000 ppm, 7000 ppm and 9000 ppm, were used in this

work to determine the surface adsorption equilibrium constant  $k$  in Eq. (5). The equilibrium adsorption amount of DBT on the surface of the porous  $\gamma$ -Al<sub>2</sub>O<sub>3</sub> was calculated by subtracting the amount of DBT in the solution in the pores from the total amount of DBT washed out of the porous  $\gamma$ -Al<sub>2</sub>O<sub>3</sub> pellets. The relationship between DBT amount adsorbed on the surface of porous Al<sub>2</sub>O<sub>3</sub> pores ( $q$ ) and the solute (DBT) concentration ( $C$ ) of equilibrium-adsorption solution in  $\gamma$ -Al<sub>2</sub>O<sub>3</sub> pores are shown by Fig. S1~Figure S5 in Supporting Information. The surface equilibrium adsorption amount of DBT is linearly proportional to its concentration in adsorption solution, being consistent with the assumption made in the model

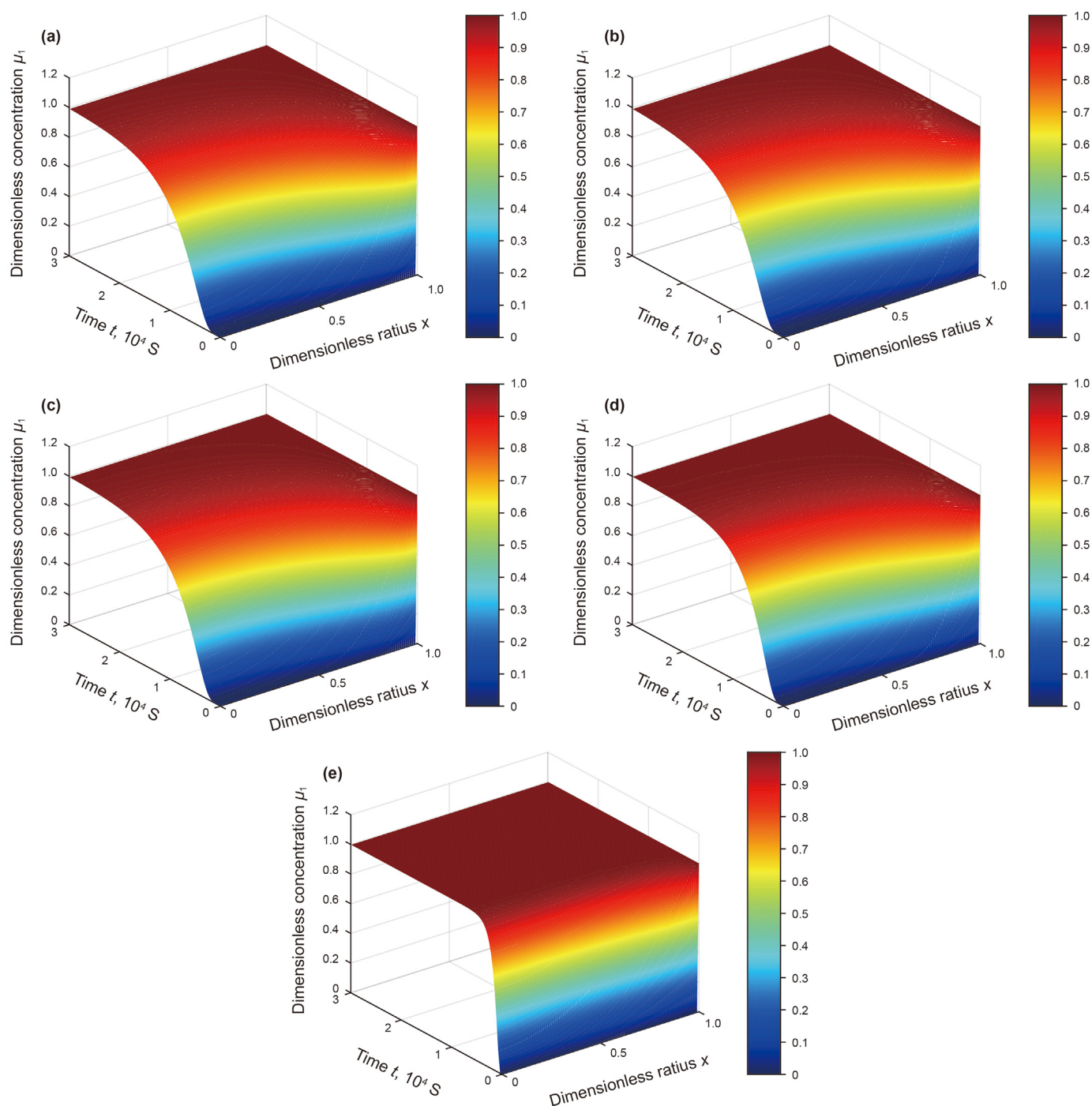


**Fig. 6.** The solute concentration distributions of the solution in porous solid pellets at different times ((a)– Al<sub>2</sub>O<sub>3</sub>-0%F; (b)– Al<sub>2</sub>O<sub>3</sub>-1%F; (c)– Al<sub>2</sub>O<sub>3</sub>-2%F; (d)– Al<sub>2</sub>O<sub>3</sub>-3%F; (e)– Al<sub>2</sub>O<sub>3</sub>/SiO<sub>2</sub> Opal).

derivation section 2. The surface adsorption equilibrium constant  $k$  is the slope of the line and summarized in Table 2 for different porous  $\gamma$ - $\text{Al}_2\text{O}_3$  pellets.

Table 2 shows that  $\text{Al}_2\text{O}_3/\text{SiO}_2$  Opal had different surface adsorption equilibrium constant  $k$  from the  $\text{Al}_2\text{O}_3$  pellets, indicating that notwithstanding the  $\text{Al}_2\text{O}_3$ -modified  $\text{SiO}_2$  had similar surface acid properties to  $\text{Al}_2\text{O}_3$  (Zhou et al., 2013), they got different surface adsorption properties. Table 2 also shows that the  $\text{Al}_2\text{O}_3$  catalysts prepared using different amounts of fibers as template had similar  $k$  values.

The measurements of effective diffusion coefficient were performed using the diffusion solution with 5000 ppm DBT. The experimental adsorption uptake rate  $((M_t/M_\infty)_{\text{exp}})$  was obtained through first measuring the uptake  $(M_t)$  at different times and the equilibrium uptake  $(M_\infty)$ , and then calculating the  $M_t/M_\infty$ . The theoretical adsorption uptake  $((M_t/M_\infty)_{\text{calc}})$  is calculated with Eq. (12) based on the numerical solution of partial differential equation of Eq. (8). The effective diffusion coefficient  $D_e$  was obtained through the parameter  $D_e$  optimization to minimize the sum of the squared difference between  $(M_t/M_\infty)_{\text{exp}}$  and  $(M_t/M_\infty)_{\text{calc}}$ . That is, the  $D_e$  was obtained through solving following optimization problem.

$$\min J = \sum_i \left( \frac{M_{t_i}}{M_\infty} \right) \left( \frac{M_{t_i}}{M_\infty} \right) \left( \frac{M_{t_i}}{M_\infty} \right) \left( \frac{M_{t_i}}{M_\infty} \right)_{\text{calc}} \Big]^2 \quad (13)$$

The good agreement between  $(M_t/M_\infty)_{\text{exp}}$  and  $(M_t/M_\infty)_{\text{calc}}$  (see Figure S.6–Figure S.10 in the Supporting Information) indicates the obtained  $D_e$  values are reliable. The  $D_e$  values of different porous solid pellets are listed in Table 3 and the solute dimensionless concentration distributions of the diffusion solution in porous solid pellets are shown in Fig. 6.

As shown in Table 3, the effective diffusion coefficient of the reference porous solid is much greater than that of conventional  $\text{Al}_2\text{O}_3$ , owing to its larger, less tortuous and more communicated pores than  $\text{Al}_2\text{O}_3$ . Although the pore structure parameters of  $\text{Al}_2\text{O}_3$  pellets obtained by  $\text{N}_2$ -adsorption desorption method are very similar to each other (Table 1), their effective diffusion coefficient increased with the amount fibers used (Table 3), for the fibers made the  $\text{Al}_2\text{O}_3$  pellet's pores being more communicated as shown in Fig. 7.

The tortuosity of the model catalyst was calculated with Eq. (3) and was found to be 1.51, closing to the theoretical value of  $\pi/2$  (Sun

**Table 4**

The pore diffusion factors of different porous solid pellets.

Catalysts	$\beta$
$\text{Al}_2\text{O}_3$ -0%F	0.123
$\text{Al}_2\text{O}_3$ -1%F	0.134
$\text{Al}_2\text{O}_3$ -2%F	0.152
$\text{Al}_2\text{O}_3$ -3%F	0.162
$\text{Al}_2\text{O}_3/\text{SiO}_2$ Opal	0.662

et al., 2019). Based on the experimental data in Tables 1 and 3, the pore diffusion factor  $\beta$  values were calculated using Eq. (4) and are listed in Table 4.

The largest value of the pore diffusion factor  $\beta$  is 1, when the pore size is large enough ( $f = 1$ , for free diffusion) and the pore is straight ( $\tau = 1$ ). Although the pores of the reference porous solid is large enough, owing to their bending, the model catalyst's  $\beta$  is smaller than 1. As shown in Table 4, the  $\beta$  of the conventional porous  $\text{Al}_2\text{O}_3$  is much smaller than 1 and smaller than that of the reference porous solid, indicating that there is lot of room for improving the diffusion ability of the conventional porous  $\text{Al}_2\text{O}_3$ . When small amount of fibers was used as template during porous  $\text{Al}_2\text{O}_3$  forming, although the low temperature  $\text{N}_2$  adsorption-desorption method cannot tell the pore structure difference, the pore diffusion factor  $\beta$  was increased significantly.

Our previous research works showed that when 3 wt% of fibers was used as the template during the forming of  $\text{Al}_2\text{O}_3$  catalyst support, the hydrodesulfurization (HDS) activity of  $\text{MoNi}/\text{Al}_2\text{O}_3$  was increased significantly (Chen et al., 2013; Fan, 2019). Small amount fibers made the pores of HDS catalysts communicated and increased the internal diffusion ability of the catalysts, resulting in the high HDS activity of the catalyst. Those HDS experiment results can be well explained by the  $\beta$  values of the hydrodesulfurization catalysts. The  $\beta$  is a very useful parameter for the evaluation of porous solid materials internal diffusion ability.

## 5. Conclusions

Although there are many methods to characterize the pore structure of solid materials, no method can characterize or measure the internal pore diffusion ability of solid materials due to their ununiform pore size and the hardly measurable pore's tortuosity. A pore diffusion factor ( $\beta$ ) was proposed to evaluate the diffusion ability of porous solid materials, and a method was proposed to measure the  $\beta$  using a well-defined and uniform pore size materials as a reference. The  $\beta$  measurement can be performed at room temperature and atmospheric pressure. The  $\beta$  can very well characterize the pore diffusion ability of porous materials. In addition, it was shown the  $\beta$  value of the porous materials was much smaller than 1, indicating that there is lot of room for improving the diffusion ability of conventional catalysts and adsorbents. Small number of fibers used as template in the porous material's forming could increase the pore diffusion factor significantly.

## Acknowledgement

This research work was supported by the National Nature Science Foundation of China (Grant No: 91534120).

## Appendix A. Supplementary data

Supplementary data to this article can be found online at <https://doi.org/10.1016/j.petsci.2022.04.008>.

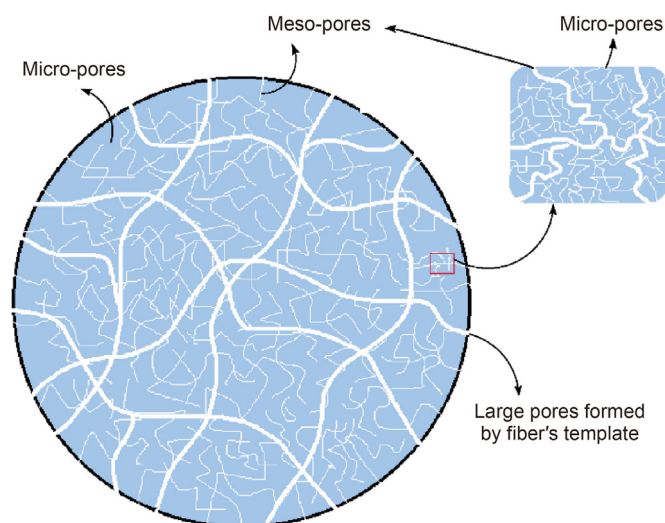


**Fig. 7.** The pore structure of  $\text{Al}_2\text{O}_3$  pellets formed using fibers as template (The fibers made the  $\text{Al}_2\text{O}_3$  pellets pores more communicated).

## References

- Absi-Halabi, M., Stanislaus, A., Al-Mughni, T., Khan, S., Qamra, A., 1995. Hydro-processing of vacuum residues: relation between catalyst activity, deactivation and pore size distribution. *Fuel* 74 (8), 1211–1215. [https://doi.org/10.1016/0016-2361\(94\)00042-P](https://doi.org/10.1016/0016-2361(94)00042-P).
- Beck, R.E., Schultz, J.S., 1970. Hindered diffusion in microporous membranes with known pore geometry. *Science* 170 (3964), 1302–1305. <https://doi.org/10.1126/science.170.3964.1302>.
- Chang, J., Liu, J., Li, D., 1998. Kinetics of residue hydrotreating reactions. *Catal. Today* 43 (3–4), 233–239. [https://doi.org/10.1016/S0920-5861\(98\)00152-7](https://doi.org/10.1016/S0920-5861(98)00152-7).
- Chen, S.L., 1998. Preparation of monosize silica spheres and their crystalline stack. *Colloids Surf. A Physicochem. Eng. Asp.* 142 (1), 59–63. [https://doi.org/10.1016/S0927-7757\(98\)00276-3](https://doi.org/10.1016/S0927-7757(98)00276-3).
- Chen, S.L., Dong, P., Xu, K., Qi, Y., Wang, D., 2007. Large pore heavy oil processing catalysts prepared using colloidal particles as templates. *Catal. Today* 125 (3), 143–148. <https://doi.org/10.1016/j.cattod.2007.02.026>.
- Chen, S.L., Dong, P., Yang, G.H., Yang, J.J., 1996. Characteristic aspects of formation of new particles during the growth of monosize silica seeds. *J. Colloid Interface Sci.* 180, 237–241. <https://doi.org/10.1006/jcis.1996.0295>, 1996.
- Chen, S.L., Feng, J., Yuan, G., Ji, Z., 2013. Preparation of Hydrodesulfurization Catalyst-Supports and Catalysts with Communicated Large and Meso Pores. *CN Patent. ZL 201110197778.2*.
- Chen, Y.W., Tsai, M.C., Li, C.P., Kang, B.C., 1994. Effect of restrictive diffusion on hydrodesulfurization of heavy residue oils over Co-Mo/Al<sub>2</sub>O<sub>3</sub>. *Can. J. Chem. Eng.* 72 (5), 854–861. <https://doi.org/10.1002/cjce.5450720512>.
- Comiti, J., Renaud, M., 1989. A new model for determining mean structure parameters of fixed beds from pressure drop measurements: application to beds packed with parallel epipedal particles. *Chem. Eng. Sci.* 44 (7), 1539–1545. [https://doi.org/10.1016/0009-2509\(89\)80031-4](https://doi.org/10.1016/0009-2509(89)80031-4).
- Fan, T., 2019. Preparation of Ni-Mo/Al<sub>2</sub>O<sub>3</sub> Catalyst with Large and Communicated Pores and its Catalytic Performance in Hydrodesulfurization Reaction, Master Thesis. China University of Petroleum-Beijing.
- Fogler, H.S., 2006. *Element of Chemical Reaction Engineering*, fourth ed. Prentice Hall, Publisher, p. 815. [https://doi.org/10.1016/0009-2509\(87\)80130-6](https://doi.org/10.1016/0009-2509(87)80130-6).
- Gao, C., Pan, Y., Zhu, B., 1997a. The determination of tortuosity factors of the silver catalyst of ethylene oxidation to ethylene oxide by steady state method. *J. Jilin Inst. Chem. Technol.* 14 (2), 1–5.
- Gao, C., Zhu, Y., Li, S., Pan, Y., Zhu, B., 1997b. The determination of tortuosity factors of the silver catalyst of ethylene oxidation to ethylene oxide by SPSR dynamic method. *J. Jilin Inst. Chem. Technol.* 14 (3), 8–13.
- ISO/TC 24/SC 4 Particle characterization, 2006. ISO 15901-2:2006: Pore Size Distribution and Porosity of Solid Materials by Mercury Porosimetry and Gas Adsorption – Part 2: Analysis of Mesopores and Macropores by Gas Adsorption, 2006–12. <https://www.iso.org/standard/39386.html>.
- ISO/TC 24/SC 4, ISO 15901-3:2007, 2007. Particle Characterization, Pore Size Distribution and Porosity of Solid Materials by Mercury Porosimetry and Gas Adsorption – Part 3: Analysis of Micropores by Gas Adsorption. <https://www.iso.org/standard/40364.html>.
- Kobayashi, S., Kushiya, S., Aizawa, R., 1987. Kinetic study on the hydro treating of heavy oil. 2. Effect of catalyst pore size. *Ind. Eng. Chem. Res.* 26 (11), 2245–2250. <https://doi.org/10.1021/ie00071a013>.
- Li, C., Chen, Y.W., Tsai, M.C., 1995. Highly restrictive diffusion under hydrotreating reactions of heavy residue oils. *Ind. Eng. Chem. Res.* 34 (3), 898–905. <https://doi.org/10.1021/ie00042a024>.
- Liu, X., 1990. *Analysis and Characterization of Industrial Catalysts*, first ed. China Petrochemical Press, Beijing, p. P85.
- Neves, C.V., Modenes, A.N., Scheufele, F.B., Rocha, R.P., Pereira, M.F.R., Figueiredo, J.L., Borba, C.E., 2021. Dibenzothiophene adsorption onto carbon-based adsorbent produced from the coconut shell: effect of the functional groups density and textural properties on kinetics and equilibrium. *Fuel* 292, 120354. <https://doi.org/10.1016/j.fuel.2021.120354>.
- Peng, P., Stolic, D., Liu, X.-M., Yan, Z.-F., Mintova, S., 2020. Strategy towards enhanced performance of zeolite catalysts: raising effective diffusion coefficient versus reducing diffusion length. *Chem. Eng. J.* 385, 123800. <https://doi.org/10.1016/j.cej.2019.123800>.
- Rao, A., Kumar, A., Dhodapkar, R., Pal, S., 2021. Adsorption of five emerging contaminants on activated carbon from aqueous medium: kinetic characteristics and computational modeling for plausible mechanism. *Environ. Sci. Pollut. Res.* 28 (17), 21347–21358. <https://doi.org/10.1007/s11356-020-12014-1>.
- Renkin, E.M., 1954. Filtration, diffusion, and molecular sieving through porous cellulose membranes. *J. Gen. Physiol.* 38 (2), 225–243. <https://doi.org/10.1085/jgp.38.2.225>.
- Sun, W., Chen, S.L., Xu, M., Wei, Y., Fan, T., Huang, L., Ma, B., Guo, J., 2019. The measurements of the intrinsic diffusivity in pores and surface diffusivity inside the porous materials in liquid phase. *Chem. Eng. Sci.* 196, 176–187. <https://doi.org/10.1016/j.ces.2018.11.006>.
- Wang, Z., Chen, S.L., Pei, J., Chen, A., Benziger, J.B., Zhang, J., Xu, Z., 2014. Insight into the intraparticle diffusion of residue oil components in catalysts during hydrodesulfurization reaction. *AIChE J.* 60 (9), 3267–3275. <https://doi.org/10.1002/aic.14501>.
- Wyllie, M.R.J., Gregory, A.R., 1955. Fluid flow through unconsolidated porous aggregates. *Ind. Eng. Chem.* 47 (7), 1379–1388. <https://doi.org/10.1021/ie50547a037>.
- Zhou, Z., Chen, S.L., Hua, D., Wang, Z., Chen, A., Wang, W., 2013. Tailored ordered porous alumina with well-defined and uniform pore-structure. *Chem. Eng. J.* 223, 670–677. <https://doi.org/10.1016/j.cej.2013.01.024>.